Accepted Manuscript

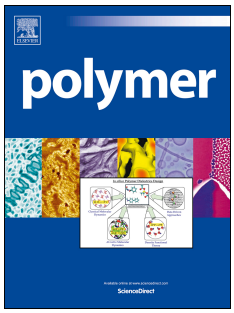

Synthesis and photovoltaic application of low-bandgap conjugated polymers by incorporating highly electron-deficient pyrrolo[3,4-*d*]pyridazine-5,7-dione units

Guobing Zhang, Jie Zhang, Guanqun Ding, Jinghua Guo, Hongbo Lu, Longzhen Qiu, Wanli Ma

PII: S0032-3861(16)30278-6

DOI: 10.1016/j.polymer.2016.04.011

Reference: JPOL 18598

To appear in: *Polymer*

Received Date: 7 January 2016

Revised Date: 14 March 2016

Accepted Date: 8 April 2016

Please cite this article as: Zhang G, Zhang J, Ding G, Guo J, Lu H, Qiu L, Ma W, Synthesis and photovoltaic application of low-bandgap conjugated polymers by incorporating highly electron-deficient pyrrolo[3,4-*d*]pyridazine-5,7-dione units, *Polymer* (2016), doi: 10.1016/j.polymer.2016.04.011.

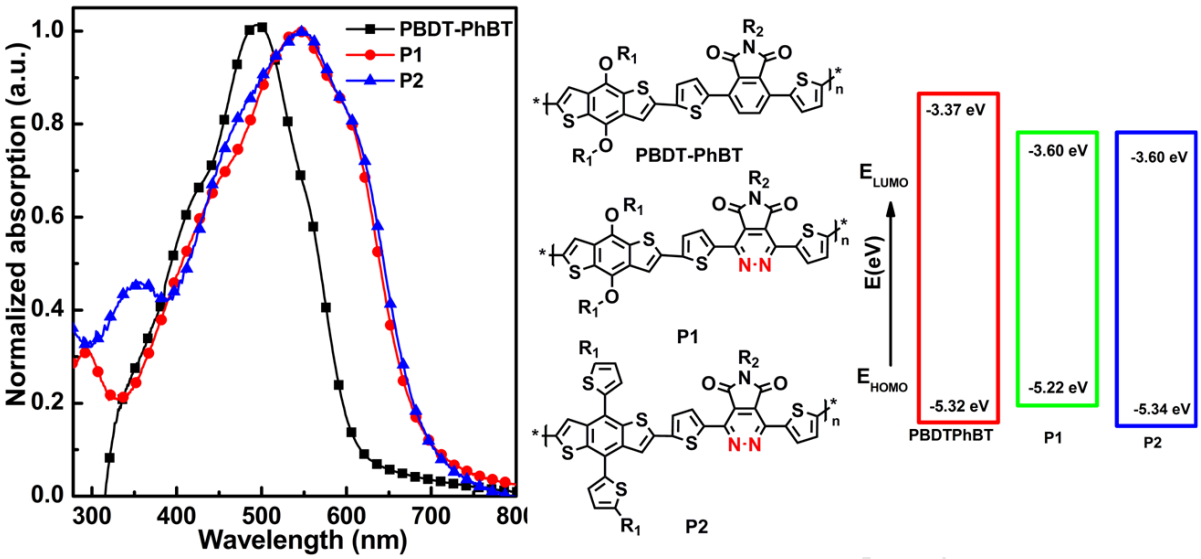

Synthesis and photovoltaic application of low-bandgap conjugated polymers by incorporating highly electron-deficient pyrrolo[3,4-*d*]pyridazine-5,7-dione units

Guobing Zhang [a, c, d, *], Jie Zhang [a, c], Guanqun Ding [b], Jinghua Guo [a, c], Hongbo Lu [a, c, d], Longzhen Qiu [a, c, d*], Wanli Ma [b,*]

[a] Key Lab of Special Display Technology, Ministry of Education, National Engineering Lab of Special Display Technology, State Key Lab of Advanced Display Technology, Academy of Opto-Electronic Technology, Hefei University of Technology, Hefei, 230009, China. E-mail: gbzhang@hfut.edu.cn

[b] Institute of Functional Nano & Soft Materials (FUNSOM), Soochow University, 199 Ren-Ai Road, Suzhou Industrial Park, Suzhou, Jiangsu 215123, P. R. China. E-mail: wlma@suda.edu.cn

[c] Department of Polymer Science and Engineering, School of Chemistry and Chemical Engineering, Hefei University of Technology, Hefei, 230009, China

[d] Anhui Key Laboratory of Advanced Functional Materials and Devices, Anhui Province, China

Abstract

Two donor–acceptor polymer semiconductors based on highly electron-deficient pyrrolo[3,4-*d*]pyridazine-5,7-dione unit were synthesized by Stille cross-coupling polymerization, and their thermal property, photophysical property, electrochemical property, microstructure, application as organic thin-film transistors, and photovoltaic property were investigated. Because of the strong electron-accepting characteristic of pyrrolo[3,4-*d*]pyridazine-5,7-dione, the new polymers (**P1** and **P2**) exhibited much wider absorption, smaller bandgaps (1.70 vs 1.98 eV), and deeper LUMO levels (–3.60 vs –3.37 eV) than those of a phthalimide-based polymer **PBDT-PhBT** (Figure 1). The fabricated organic thin-film transistor devices exhibited hole-transport behavior, and the highest mobility of 1.14×10^{-3} $cm^2V^{-1}s^{-1}$ was obtained. The bulk-heterojunction solar cells based on the two polymers as the electron donors and $PC_{71}BM$ as the electron acceptor showed a high open-circuit voltage and achieved a power conversion efficiency of 2.71% and 3.66% for polymers **P1** and **P2**,

respectively. This is the first report on photovoltaic performances of pyrrolo[3,4-*d*]pyridazine-5,7-dione-based polymers.

Key words: Pyrrolo[3,4-*d*]pyridazine-5,7-dione Low bandgap Polymer solar cells

1. Introduction

Over the past decade, polymer solar cells (PSCs) have attracted tremendous attention owing to their significant advantages of low cost, light weight, large area, flexibility, and application as environmentally friendly energy-converting devices [1-9]. So far, the bulk hetero-junction (BHJ)-type PSCs based on the blending of electron-donating conjugated polymers and high-electron-affinity fullerene derivatives have become the most successful device structure for PSCs [10-12]. Power conversion efficiency (PCE) is the product of the short-circuit current density (Jsc), open-circuit voltage (Voc), and fill factor (FF) divided by the incoming light power density. The established design rules for electron donor conjugated polymers in fullerene-based BHJ devices are as follows: a low level of the highest occupied molecular orbital (HOMO) for a high Voc, a low bandgap for a large solar photon harvest, a suitable energy offset between the lowest unoccupied molecular orbital (LUMO) of the electron donor polymer and that of the fullerene for efficient charge separation [13-16]. As one of the building units in conjugated copolymers, phthalimide (Ph) unit has attracted much interest because of its inherent advantages. Phthalimide can be easily synthesized and has a symmetric, rigidly fused, and coplanar structure, which can facilitate the electron delocalization when incorporated into conjugated polymers [17, 18]. Moreover, its relatively high electron-withdrawing ability would lead to lower HOMO energy levels (approximately from –5.2 to –5.4 eV) of the conjugated polymers. Usually, a lower HOMO energy level is beneficial to obtain a higher Voc of PSCs [17, 19]. Phthalimide-based conjugated polymers have been widely explored for organic electronic applications and shown high mobility in organic thin-film transistors (OTFTs) [20]. However, phthalimide-based donor–acceptor (D–A) polymers have relatively high LUMO levels and thus exhibit a wide bandgap (Eg > 2 eV), which

adversely effects the solar photon harvest. Moreover, an energy difference between the LUMOs (donor/PCBM) is larger than the minimum value (~0.3 eV) may not be advantageous, and indeed wastes energy that does not contribute to the device performance [11, 21-22]. Further improvement of phthalimide-based polymers by reducing the bandgap while maintaining a low HOMO level is needed for fully exploring their potential as low-bandgap polymers for PSCs applications. Previous studies indicate that the HOMO level of D–A polymers was determined by the electron-donor unit, whereas the LUMO level was mainly controlled by the electron-acceptor unit [23, 24]. Therefore, the incorporation of a more electron-deficient acceptor to lower the LUMO level, which would result in a smaller bandgap and maintain a low HOMO level, may be an efficient method.

Compared to benzene, pyridazine is highly electron deficient. If the pyrrolo[3,4-*d*]pyridazine-5,7-dione unit is introduced into D–A polymers by replacing the benzene ring of Ph with pyridazine, the polymers would have lower LUMO energy and smaller bandgap than the phthalimide-based polymers [25, 26]. In this study, this strategy was applied. Herein, we reported the synthesis and characterization of two D–A polymers (Figure 1, polymers **P1** and **P2**) using highly electron-deficient pyrrolo[3,4-*d*]pyridazine-5,7-dione as the electron acceptor and benzodithiophene (BDT) as the electron donor. Consequently, compared to polymer PBDT-PhBT, polymers **P1** and **P2** exhibited much wider absorptions, much smaller bandgaps, lower LUMO levels, and similar deep HOMO levels. The hole-transport and photovoltaic performances with polymers **P1** and **P2** as electron donors and PCBM as the electron acceptor were also investigated.

2. Experimental part

2.1 Material and instruments

All chemicals were purchased from commercial suppliers and used without further purification. Toluene was distilled over sodium under nitrogen prior to use. 2,6-Bis(trimethylstannyl)-4,8-bis(2-ethylhexyloxy)benzol[1,2-b:4,5-b’]dithiophene and 2,6-bis(trimethyltin)-4,8-bis(5-(2-ethylhexyl)thiophene-2-yl)benzol[1,2-b:4,5-b’]-

dithiophene was purchased from Suna Tech Inc. Monomer **1**-**3** and **M** were prepared according to the literature [25, 26]. The ^{1}H NMR spectra were recorded by a VNMRS600 MHz spectrometer. The molecular weights of the polymers were measured by GPC using a Waters Series 1525 gel at 100 ^{o}C, and 1,2,4-trichlorobenzene was used as eluent and polystyrene as the standard. The thermal analyses were performed on a TA instrument QS000IR under a nitrogen atmosphere and a heating rate of 10 °C/min. DSC measurements were conducted under nitrogen on a TA Instruments Q2000, and the samples were heated at a rate of 10 °C/min. The UV–visible absorption spectra were obtained from a Perkin Elmer model UV–visible spectrophotometer. The cyclic voltammetry (CV) was performed on a CHI 660D electrochemical workstation equipped with a three-electrode system in an acetonitrile solution of 0.1 M Bu_4NPF_6 and at a scan rate of 100 mV/s. Ferrocene was used as the standard, and the polymer thin films were coated on a platinum disc electrode, which was used as the working electrode. A platinum wire was used as the auxiliary electrode, and an Ag/Ag^{+} electrode was used as the reference electrode. The morphology of the polymer films was investigated using a Veeco Multimode V AFM in tapping mode equipped with a 1 μm scanner.

2.2 Fabrication and characterization of polymer solar cells

PSCs were fabricated with a general structure of ITO/PEDOT-PSS (40 nm)/ polymer: PCBM/LiF/Al. Patterned ITO glass substrates were cleaned by sequential ultrasonic treatment in detergent, isopropyl alcohol and acetone, and the organic residue was further removed by treating with UV-ozone for 15 min. ITO substrates were spin-coated with a thin film about 40 nm of PEDOT:PSS and dried at 150 ^{o}C for 10 min. A blend of polymer and PCBM was solubilized in chloroform solvent with or without DIO, filtered through a 0.45 mm poly(tetra-uoroethylene) (PTFE) filter, spin-coated at different rpm (1500 rpm) for 40 s, 0.6 nm of LiF (0.1 A s^{-1}) and 100 nm Al (2 A s^{-1}) layers were then thermally evaporated on the active layer at a pressure of 1.0×10^{-6} mbar through a shadow mask (active area 72.5 mm^2). The current–voltage characteristics of the photovoltaic cells were measured on a Keithley 2400 (*I*–*V*)

Digital source meter under one sun of simulated air mass 1.5G (AM 1.5G) solar irradiation of 100 mW/cm^2 (Newport Stratford, Inc., 94023A).

2.3 Fabrication and characterization of field-effect transistors

The hole transport properties of the two polymers were investigated using a bottom-gated/top-contact OTFTs configuration, with a 300-nm-thick SiO_2 dielectric on a heavily *N*-type-doped silicon substrate as the gate electrode. A fluoropolymer Cytop was spin-coated to reduce the number of hydroxyl groups present on the SiO_2 surface. The organic semiconductor thin films were prepared by spin-coating of a 5 mg/mL chloroform solution at 8000 rpm. The polymer films were subsequently annealed at 180 °C for 30 min in a nitrogen-filled glove box. Then, the Au source/drain electrodes were evaporated on top of these semiconductor layers (40 nm). The OTFTs devices had a channel length (L) of 100 μm and a channel width (W) of 800 μm. The OTFTs measurements were carried out under ambient environment using a Keithley 4200-SCS semiconductor parametric analyzer on the probe stage. The mobilities of holes (μ_h) were obtained from the following equation at the saturation regime: $I_d = (W/2L)C_i\mu(V_g - V_{th})^2$, where W/L is the channel width/length, I_d is the drain current in the saturated regime, C_i is the capacitance of the Cytop gate dielectric, and V_{th} is the threshold voltage.

2.4 **Synthesis**

2.4.1 Synthesis of P1

$Pd_2(dba)_3$ (0.0072 g, 0.0079 mmol), P(*o*-tolyl)$_3$, (0.0096 g, 0.032 mmol), 2,6-bis(trimethyltin)-4,8-bis(2-ethylhexyloxy)benzo[1,2-*b*:4,5-*b*']dithiophene (0.152 g, 0.20 mmol) and1,4-bis(5-bromothiophene-2-yl)-6-decyltetradecyl-5H-pyrrolo[3,4-*d*]pyridazine-5, 7-dione (0.159 g, 0.20 mmol) were mixed in toluene (8 mL). The solution was subjected to three cycles of admission and evacuation of nitrogen before heated to 105 ℃ for 48h.After cooled to room temperature, methanol and HCl were added and stirred for 2 h. The precipitate was collected by filtration. The product was purified by washing with methanol and dichloromethane in a Soxhlet extractor for 24 h each. It

was extracted with hot chloroform in an extractor for 24 h. After removing solvent, the purple solid was collected (0.14 g, 62.9%). ^{1}H NMR (600 MHz, $CDCl_3$, ppm): δ = 8.45–8.95 (br, 2H), 6.28–7.21 (br, 4H), 3.54–4.59 (br, 6H), 0.99–2.10 (br, 56H), 0.60–0.95 (br, 18H). Anal. calcd for $C_{64}H_{91}N_3O_4S_4$ (%): C, 70.22, H, 8.38, N, 3.84, found (%) C, 70.06, H, 8.56, N, 3.68.

2.4.2 Synthesis of P2

The same procedures were used as for **P1**. Compounds used were $Pd_2(dba)_3$ (0.068 g, 0.0074 mmol), P(*o*-tolyl)$_3$ (0.0090 g, 0.030 mmol), 2,6-bis(trimethyltin)-4,8-bis(5-(2-ethylhexyl)-thiophen-2-yl)benzo[1,2-*b*:4,5-*b*']dithiophene (0.17 g, 0.19 mmol), 1,4-bis(5-bromothiophene-2-yl)-6-decyltetradecyl-5H-pyrrolo[3,4-*d*]pyridazine-5,7-dione (0.15 g, 0.19 mmol). After workup, the purple solid were obtained (0.13 g, 55.1%). ^{1}H NMR (600 MHz, $CDCl_3$, ppm): δ = 8.30–8.88 (br, 2H), 6.31–7.59 (br, 8H), 3.45–4.08 (br, 2H), 2.65–3.36 (br, 4H), 0.92–2.13 (br, 56H), 0.68–0.92 (br, 18H). Anal. calcd for $C_{72}H_{95}N_3O_2S_6$ (%): C, 70.48, H, 7.80, N, 3.42, found (%) C, 70.36, H, 7.76, N, 3.35.

3. Results and discussion

3.1 Synthesis and characterization

Scheme 1 shows the syntheses of the monomers and polymers. The monomers were synthesized according to a previous literature report [25, 26]. Polymers **P1** and **P2** were synthesized by Stille cross-coupling reactions in a 1:1 monomer ratio with the presence of $Pd_2(dba)_3$ as the catalyst and P(*o*-tolyl)$_3$ as the ligand. The two polymers showed good solubility in organic solvents such as tetrahydrofuran (THF), chloroform, and chlorobenzene at room temperature. The number-average molecular weights and polydispersity indexes (PDI) of the polymers were determined by gel permeation chromatography (GPC) with trichlorobenzene as the eluent and polystyrene as the standard at a column temperature of 100 ^{o}C. The GPC plots are shown in Figure S1 and S2 (Supporting Information). The number-average molecular weights of polymers **P1** and **P2** were 12.4 kDa and 11.9 kDa with PDIs of 1.58 and 1.73, respectively.

Figure 2 shows the thermogravimetric analysis (TGA) and differential scanning calorimetry (DSC) curves of the two polymers. A weight loss of 5% was selected as the onset decomposition point. Polymers **P1** and **P2** were thermally stable up to 377 and 380 °C, respectively. The two polymers showed a good thermal stability for applications in optoelectronic devices; none of them showed significant transition in the DSC analyses.

3.2 Optical properties

The UV–visible absorption spectra of polymers **PBDT-PhBT**, **P1**, and **P2** in chloroform solutions and as thin films are shown in Figure 3. The corresponding optical data are summarized in Table 1. As shown in Figure 3a, the three polymers **PBDT-PhBT**, **P1**, and **P2** showed absorption maxima at 462, 532, and 536 nm in solutions, respectively. After the spin-coating into a thin film, the absorption bands of polymers **P1** and **P2** were broadened, and the absorption maxima of polymers **P1** and **P2** were located at 543 and 546 nm (Figure 3b), red-shifted by approximately 11 and 10 nm, respectively. The absence of strong red-shifts from the solutions to the films can be attributed to the probable preaggregation in solutions [27, 28]. The absorption spectra of polymers **P1** and **P2** covered the UV–visible region ranging from 300−730 nm, much broadened than that of polymer **PBDT-PhBT**. The edges of the film absorption bands for polymers **PBDT-PhBT**, **P1**, and **P2** were located at 627, 730, and 730 nm, respectively. The corresponding optical bandgaps of polymers **PBDT-PhBT**, **P1**, and **P2** were 1.98, 1.70, and 1.70 eV, respectively. The replacement of the phthalimide unit with the stronger electron-deficient pyrrolo[3,4-*d*]pyridazine-5,7-dione unit may result in stronger D–A interactions, which may effectively extend the absorption spectra. As a result, the corresponding polymers exhibited much smaller bandgaps.

3.3 Electrochemical properties

The electrochemical properties of the polymers were investigated by cyclic voltammetry (CV). Figure 4 shows the CVs of polymers **P1** and **P2** films on a platinum disc electrode in an acetonitrile solution containing 0.1 M Bu_4NPF_6. The

corresponding data were summarized in Table 1. The onset oxidation potentials of polymers **P1** and **P2** were 0.47 and 0.59 V, respectively, whereas the onset reduction potential of polymers **P1** and **P2** had the same value of –1.15 V. The HOMO levels of the two polymers **P1** and **P2** were calculated to be –5.22 and –5.34 eV, respectively, close to the HOMO level (–5.32 eV) of polymer **PBDT-PhBT**. A deep HOMO level should help the two polymers achieve a good stability against oxidation. The LUMO levels of the two polymers were both –3.60 eV, significantly deeper than that of polymer **PBDT-PhBT** (–3.37 eV). The low LUMO levels of the two polymers can be attributed to the strong electron-deficient pyrrolo[3,4-*d*]pyridazine-5,7-dione units in the polymer backbone. It can be concluded that the replacement of alkoxy side chains with alkylthienyl groups lowers the HOMO level, thus increasing the *V*oc of the PSCs. The electrochemical band gaps of polymers **P1** and **P2** (1.62/1.74 eV) are matched well with their optical band gaps (1.70/1.70 eV) within the experimental error.

3.4 Theoretical calculations

For better understanding of the molecular architecture of the polymers, molecular simulation was carried out for polymers **PBDT-PhBT**, **P1** and **P2** using density functional theory (DFT) at B3LYP/6-31g level with the Gaussian 09. To simplify the calculation, all the alkyl and alkoxy groups were replaced with methyl and methoxy groups, respectively. Figure 5 shows the calculated molecular orbital geometry and energy levels on the model compound of the polymers. The HOMO levels of polymers are mainly delocalized over the benzothiophene and thiophene units, therefore, the three polymers have similar deep HOMO levels. In contrast to the HOMO levels, the LUMO levels are distributed on the acceptor units. Since the pyrrolo[3,4-*d*]pyridazine-5,7-dione shows stronger electron-deficient than that of phthalimide unit, polymers **P1** and **P2** have much lower LUMO levels compared to that of **PBDT-PhBT**. This result indicates that the LUMO levels can be effectively lowered by changing the acceptor unit.

3.5 Hole mobility

The hole mobilities of pristine polymers **P1** and **P2** in films were investigated by

fabricating OTFTs with bottom-gate, top-contact configurations. The polymer films were subsequently annealed at 180 °C in a glove box under nitrogen atmosphere. The output and transfer characteristics are shown in Figure 6 and the corresponding device performances are listed in Table S1 (Supporting Information). Both polymers **P1** and **P2** showed typical hole-transport characteristics. The nonannealing (N/A) devices showed mobilities of 3.29×10^{-5} $cm^2V^{-1}s^{-1}$ for polymer **P1** and 6.13×10^{-4} $cm^2V^{-1}s^{-1}$ for polymer **P2**. Thermal annealing was beneficial to optimize the device performance, the thermally annealed thin film of polymer **P1** exhibited a hole mobility of 1.08×10^{-4} $cm^2V^{-1}s^{-1}$. Replacement of alkoxyl BDT with the alkylthienyl BDT yield a significant increase of hole transport, **P2** exhibited a hole mobility of 1.14×10^{-3} $cm^2V^{-1}s^{-1}$.

3.6 Photovoltaic performance

The photovoltaic performances of polymers **P1** and **P2** were also investigated in BHJ solar cell devices. The polymers were used as the electron donor and PCBM was used as the electron acceptor. The conventional device structure was ITO/PEDOT-PSS/polymer:PCBM/LiF/Al. The devices were characterized under AM 1.5 G illumination at 100 mW/cm^2 using a solar simulator. The device optimization was carried out using the ratio shown in Table S2. The devices with $PC_{61}BM$ as the electron acceptor were initially fabricated with different D:A blend ratios from 1:1 to 1:4. As shown in Table S2, the optimized ratio of polymer to $PC_{61}BM$ was 1:2. At the 1:2 weight ratio of polymer/$PC_{61}BM$, the device based on **P1**/$PC_{61}BM$ as the active layer afforded a V_{oc} of 0.91 V, a J_{sc} of 1.92 mA/cm^2, a FF of 47%, and a PCE of 0.83%. The device using **P2**/$PC_{61}BM$ as the active layer exhibited a V_{oc} of 0.91 V, a J_{sc} of 2.49 mA/cm^2, a FF of 46%, and a PCE of 1.04%. Additives have been widely used to optimize the morphology of BHJ PSCs, and 1,8-diiodooctane (DIO) has been reported as one of the most efficient additives [29]. Therefore, DIO was also added from 1 to 4 vol% to optimize the device performance. Table 2 shows the performances of the devices with different amounts of additive. The best PCE was achieved with 3 vol% DIO as the additive for both polymers **P1** and **P2**. The current

density-voltage (*J-V*) curves of PSCs with blends of polymers, $PC_{61}BM$, and 3 vol% DIO are shown in Figure 7. The optimized devices exhibited PCE of 1.73% and 1.84% with J_{sc} value of 3.66 and 3.74 mA/cm^2 for polymers **P1** and **P2**, respectively. The $PC_{71}BM$ was selected as the electron acceptor to further optimize the device performance. The current *J-V* curves of devices are presented in Figure 8 and the corresponding results are summarized in Table 3. The **P1**/$PC_{71}BM$ based devices displayed a PCE of 2.71% with a V_{oc} of 0.86 V and a J_{sc} of 5.96 mA/cm^2, the **P2**/$PC_{71}BM$ based devices exhibited a PCE of 3.66% with a V_{oc} of 0.91 V and a J_{sc} of 6.04 mA/cm^2. The significant increase of J_{sc} and PCE was attributed to the improvement of complementary absorption of $PC_{71}BM$ and charge separation in BHJ. The morphology of the active layer was characterized by Atomic force microscopy (AFM). The AFM topography and phase images of the film casted from the polymer/$PC_{71}BM$ blend without and with DIO additive were reordered. As shown in Figure 9, the blend films showed large aggregations when spin-coated without DIO. This could cause inefficient exciton dissociation. After addition of DIO, the aggregations in the blend films were suppressed and the domain sizes were relatively reduced. The films processed with DIO exhibited fine domains and no large phase separation was observed compared to the film processed without DIO.

The pyrrolo[3,4-*d*]pyridazine-5,7-dione-based polymers (**P1** and **P2**) exhibited moderate performances. This might be attributed to the relatively low molecular weights and unoptimized composite morphology. Also, when straight alkyl chains (dodecyl) and short branched chains (ethylhexyl) were used in pyrrolo[3,4-*d*]pyridazine-5,7-dione monomers, the resulting polymers were completely insoluble in solvent. Large branched side chains were used in the synthesis of these polymers, which efficiently improved the solubility of the resulting polymers. However, large and bulky side chains may also significantly reduce the crystallinity and hole mobility of polymers, thus causing a low device performance.

4. Conclusion

Two D–A polymers based on the pyrrolo[3,4-*d*]pyridazine-5,7-dione unit, which

replaced the benzene ring of phthalimide with pyridazine, were successfully synthesized by Stille cross-coupling polymerization. The results indicated that the replacement of the benzene ring with pyridazine significantly affected the absorption spectrum, bandgap, and LUMO level of the resulting polymers. The BHJ solar cells based on the two polymers as the electron donors and $PC_{71}BM$ as the electron acceptor achieved moderate PCE of 2.71% and 3.66% for polymers **P1** and **P2**, respectively. However, after the structure and composite morphology optimizations, polymers **P1** and **P2** exhibited wide absorptions, low bandgaps, suitable LUMO levels, and deep HOMO levels. This indicated that pyrrolo[3,4-*d*]pyridazine-5,7-dione-based D–A polymers have great potential as semiconductors in photovoltaic applications.

Acknowledgements

This work was supported by National Nature Science Foundation of China (NSFC Grant Nos. 21204017, 21174036)..

References

1. J. Chen, Y. Cao, *Acc Chem Res*, 42 (11) (2009) 1709–1718.

2. S. Günes, H. Neugebauer, N. S. Sariciftci, *Chem Rev*, 107 (4) (2007) 1324–1338.

3. A. Pershin, S. Donets, S. A. Baeurle, *Polymer*, 55 (16) (2014) 3736–3745.

4. G. Zhang, Y. Fu, L. Qiu, Z. Xie, *Polymer*, 53 (20) (2012) 4407–4412.

5. J. Peet, J. Y. Kim, N. E. Coates, W. L. Ma, D. Moses, A. J. Heeger, G. C. Bazan, *Nat Mater*, 6 (7) (2007) 497–500.

6. M. H. Hoang, D. N. Nguyen, T. T. Ngo, H. A. Um, M. J. Cho, D. H. Choi, *Polymer*, 83 (2016) 77-84.

7. X. Gong, *Polymer*, 53 (24) (2012) 5437-5448.

8. P. Shen, H. Bin, L. Chen, Z-G. Zhang, Y. Li, *Polymer*, 79 (19) (2015) 119-127.

9. J. Yuan, Z. Zhai, H. Dong, J. Li, Z. Jiang, Y. Li, W. Ma, *Adv. Funct. Mater*., 23 (7) (2013) 885-892.

10. G. Yu, J. Gao, J. C. Hummelen, F. Wudl, A. J. Heeger, *Science*, 270 (5243) (1995) 1789–1791.

11. B. C. Thompson, J. M. J. Fréchet, *Angew Chem Int Ed*, 47 (1) (2008) 58–77.

12. K. Kranthiraja, K. Gunasekar, W. Cho, M. Song, Y. G. Park, J. Y. Lee, Y. Shin, I. N. Kang, A. Kim, H. Kim, B. S. Kim, B. S. Kim, S. H. Jin, *Macromolecules*, 47 (20) (2014) 7060-7069.

13. G. Zhang, J. Yuan, P. Li, J. Ma, H. Lu, L. Qiu, W. Ma, *Polym Chem*, 4 (11) (2013) 3390–3397.

14. T. Yang, M. Wang, C. Duan, X. Hu, L. Huang, J. Peng, F. Huang, X. Gong, *Energy Environ Sci*, 5 (8) (2012) 8208–8214.

15. G. Zhang, Y. Fu, Z. Xie, Q. Zhang, *Polymer*, 52 (2) (2011) 415–421.

16. L. Ye, S. Zhang, D. Qian, Q. Wang, J. Hou, *J. Phys. Chem. C*, 117 (48) (2013) 25360-25366.

17. H. Xin, X. Guo, F. S. Kim, G. Ren, M. D. Watson, S. A. Jenekhe, *J Mater Chem*, 19 (30) (2009) 5303–5310.

18. J. Huang, X. Wang, C. Zhan, Y. Zhao, Y. Sun, Q. Pei, Y. Liu, J. Yao, *Polym Chem*, 4 (6) (2013) 2174–2182.

19. G. Zhang, Y. Fu, Q. Zhang, Z. Xie, *Macromol Chem Phys*, 211 (24) (2010) 2596–2601.

20. X. Guo, F. S. Kim, S. A. Jenekhe, M. D. Watson, *J Am Chem Soc*, 131 (21) (2009) 7206–7207.

21. L. J. A. Koster, V. D. Mihailetchi, P. W. M. Blom, *Appl Phys Lett*, 88 (9) (2006) 093511.

22. J. Huang, Y. Zhao, W. He, H. Jia, Z. Lu, B. Jiang, C. Zhan, Q. Pei, Y. Liu, J. Yao, *Polym. Chem.*, 3 (10) (2012) 2832-2841.

23. J. Chen, Y. Cao, *Acc. Chem. Res.*, 42 (11) (2009) 1709-1718.

24. H. Yao, H. Zhang, L. Ye, W. Zhao, S. Zhang, J. Hou, *ACS Appl. Mater. Interfaces*, 8 (6) (2016) 3575-3583.

25. Q. Ye, W. T. Neo, C. M. Cho, S. W. Yang, T. Lin, H. Zhou, H. Yan, X. Lu, C. Chi, J. Xu, *Org Lett*, 16 (24) (2014) 6386–6389.

26. C. M. Cho, Q. Ye, W. T. Neo, T. Lin, X. Lu, J. Xu, *Polym. Chem.*, 6 (43) (2015)

7570-7579.

27. J. Kim, A. R. Han, J. Hong, G. Kim, J. Lee, T. J. Shin, J. H. Oh, C. Yang, *Chem Mater*, 26 (17) (2014) 4933–4942.

28. N. Zhou, X. Guo, R. P. Ortiz, S. Li, S. Zhang, R. P. H. Chang, A. Facchetti, T. J. Marks, *Adv Mater*, 24 (17) (2012) 2242–2248.

29. J. K. Lee, W. L. Ma, C. J. Brabec, J. Yuen, J. S. Moon, J. Y. Kim, K. Lee, G. C. Bazan, A. J. Heeger, *J Am Chem Soc*, 130 (11) (2008) 3619–3623.

Figure Captions

Scheme 1 Synthetic routes of the monomers and polymers.

Figure 1 Molecular structures of polymers **PBDT-PhBT**, **P1**, and **P2**.

Figure 2 (a) TGA plots of copolymers at a heating rate of 10 °C/min, (b) DSC curves of the copolymers in inert atmosphere.

Figure 3 Normalized absorption spectra of copolymers (a) in solutions and (b) as thin films.

Figure 4 Cyclic voltammograms of the polymers at a scan rate of 100 mV/s.

Figure 5 Molecular orbital distribution of HOMO and LUMO for energy-minimized structure (B3LYP/6-31g*) of the model compounds.

Figure 6 Output (a, b) and transfer characteristics (c and d) of polymers **P1** and **P2** annealed at 180 °C.

Figure 7 Illuminated *I–V*curves of PSC devices based on polymers/$PC_{61}BM$ fabricated from chloroform with DIO.

Figure 8 Illuminated *I–V*curves of PSC devices based on polymers/$PC_{71}BM$ fabricated from chloroform with DIO.

Figure 9 AFM images of **P1**/$PC_{71}BM$ and **P2**/$PC_{71}BM$ with and without DIO processed from chloroform.

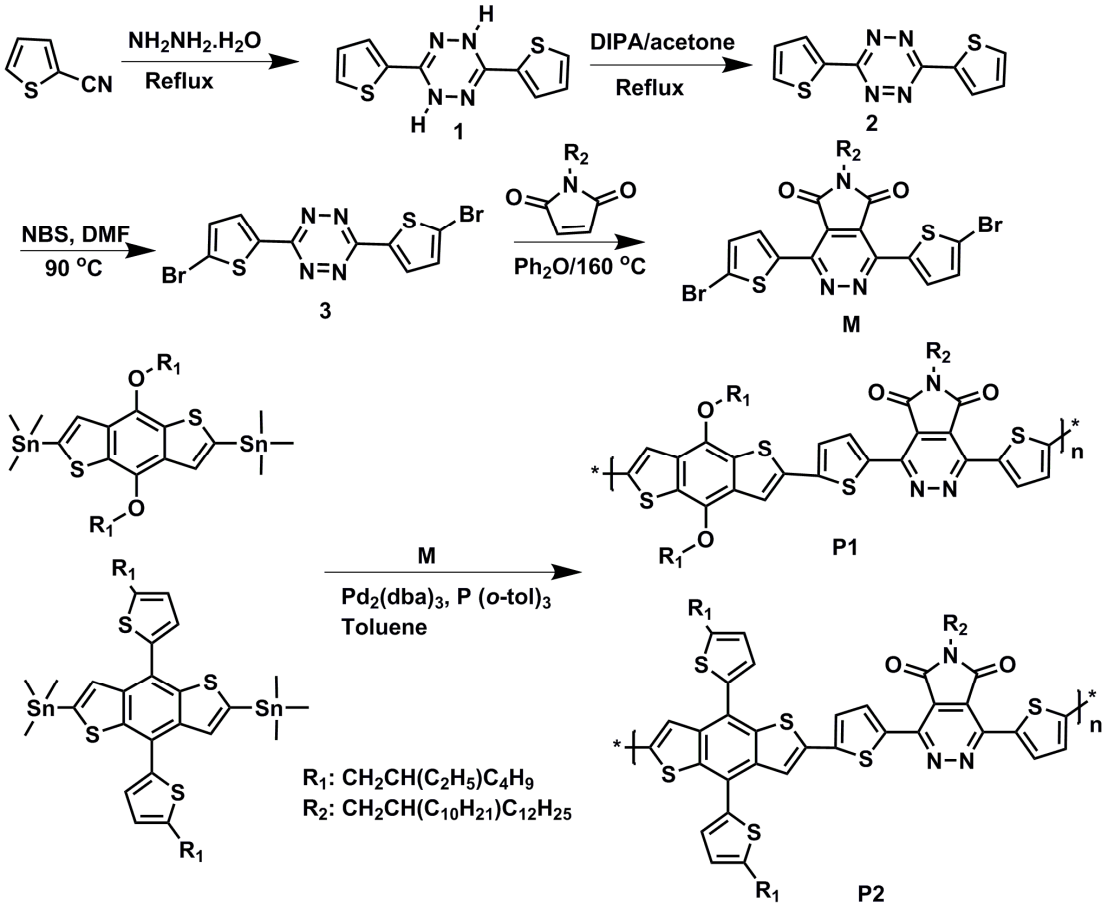

Scheme 1

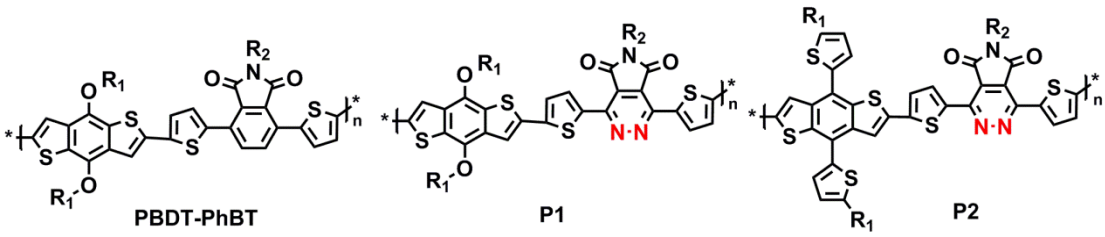

Figure 1

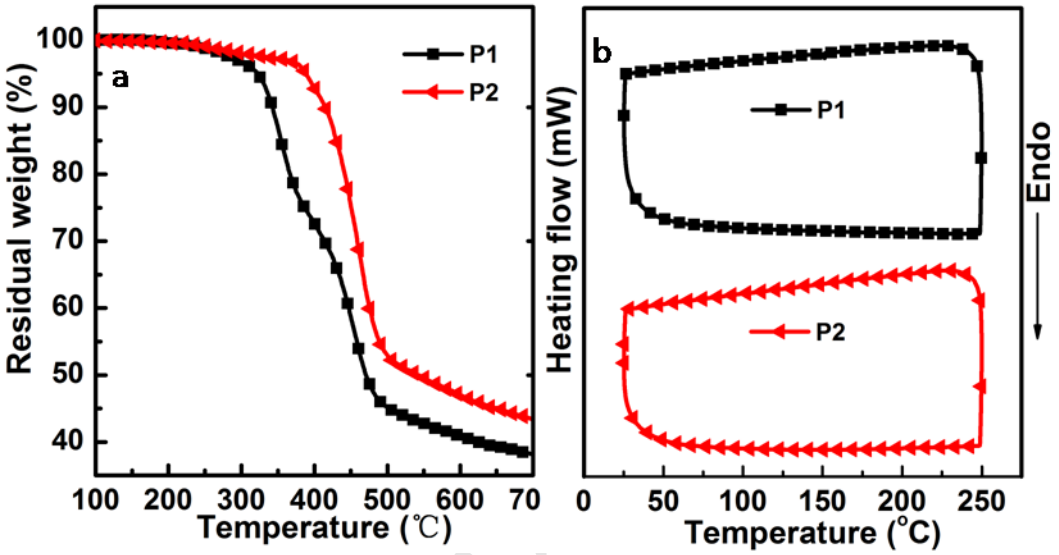

Figure 2

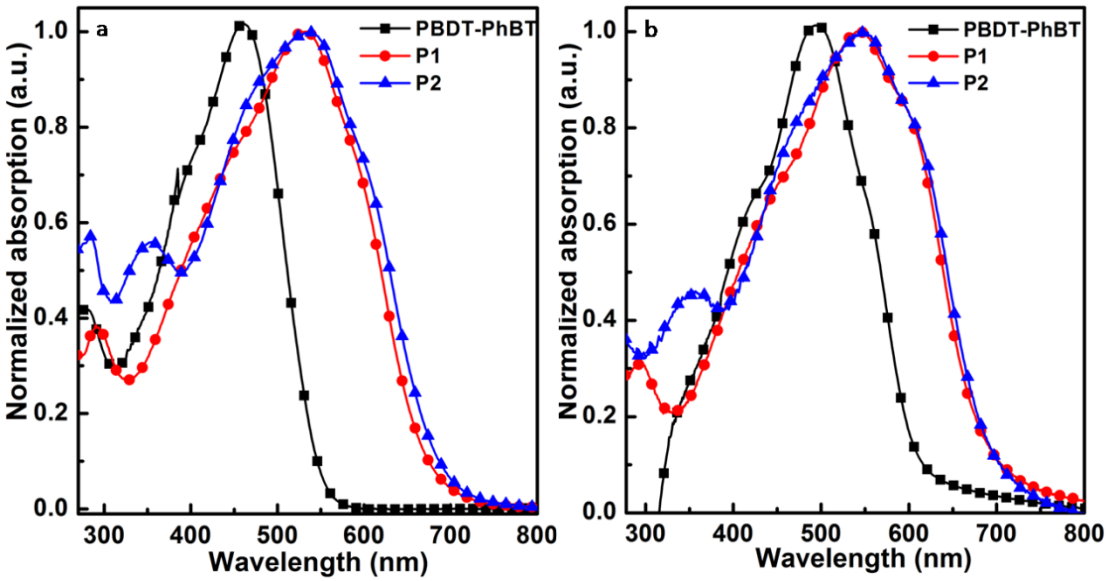

Figure 3

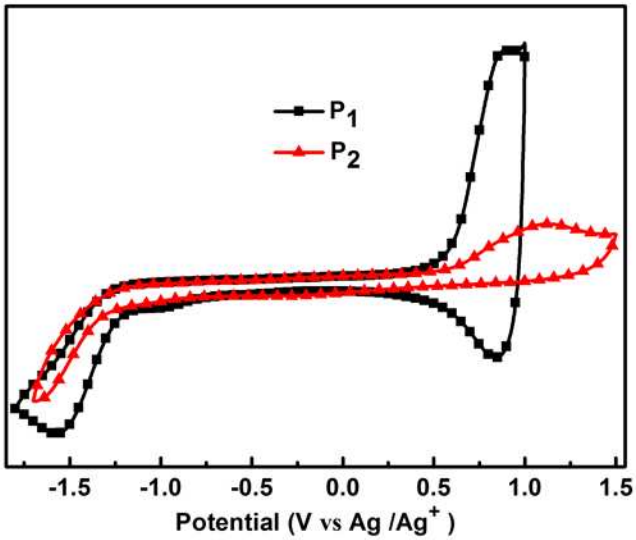

Figure 4

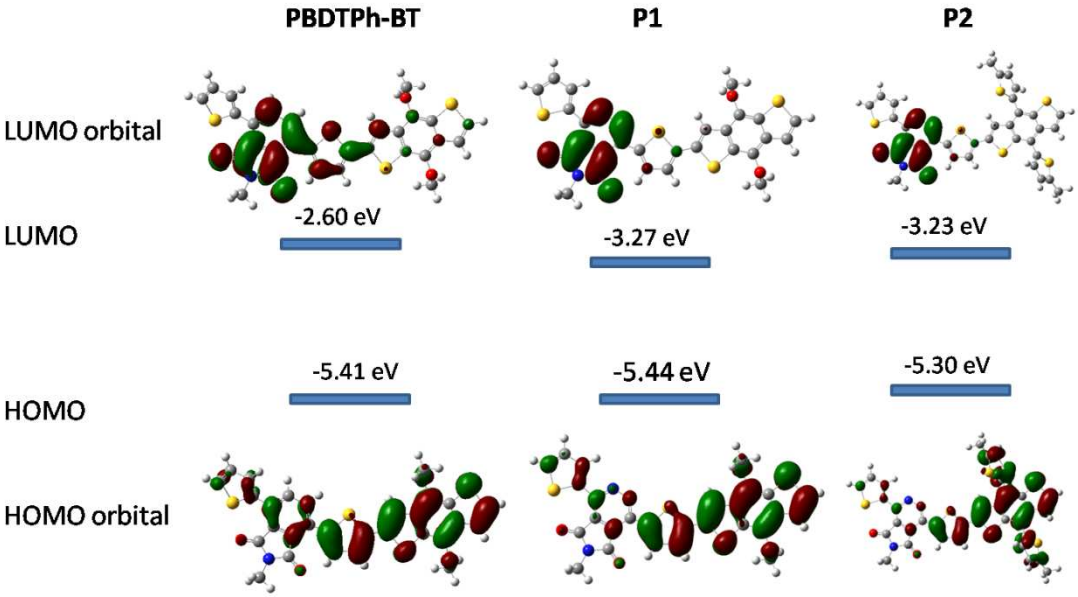

Figure 5

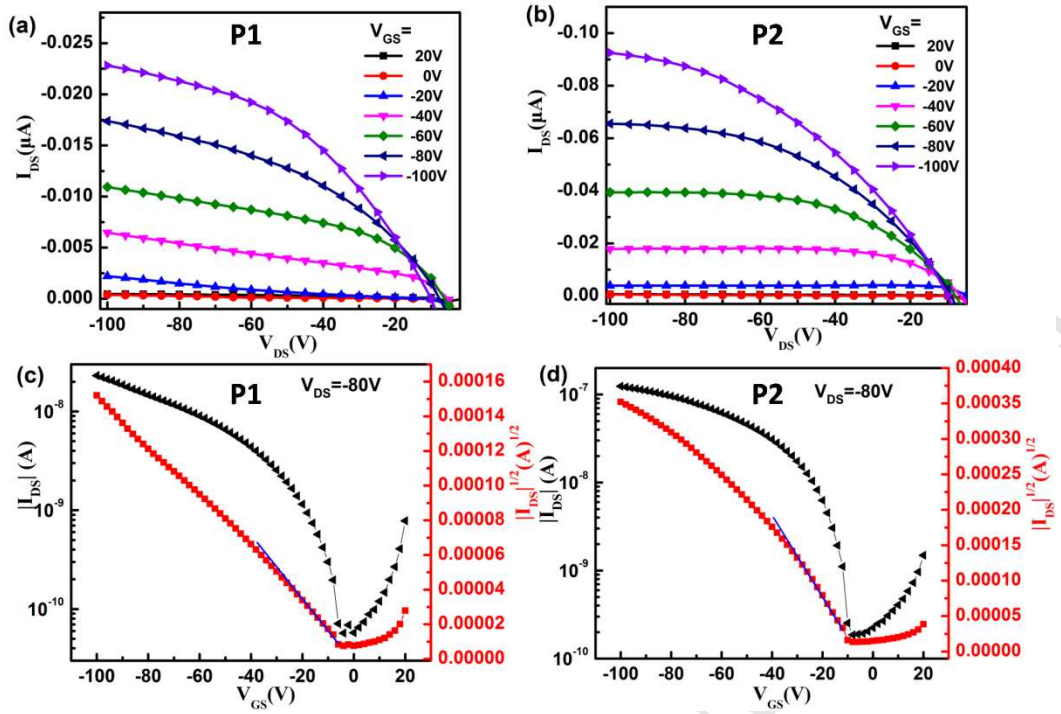

Figure 6

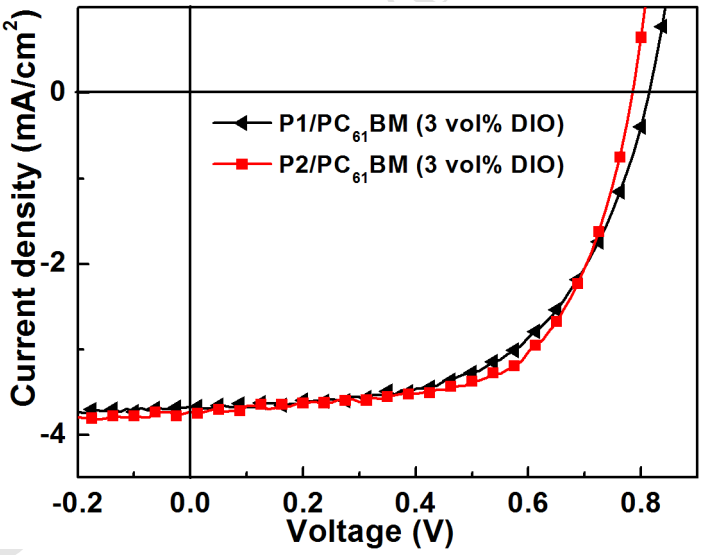

Figure 7

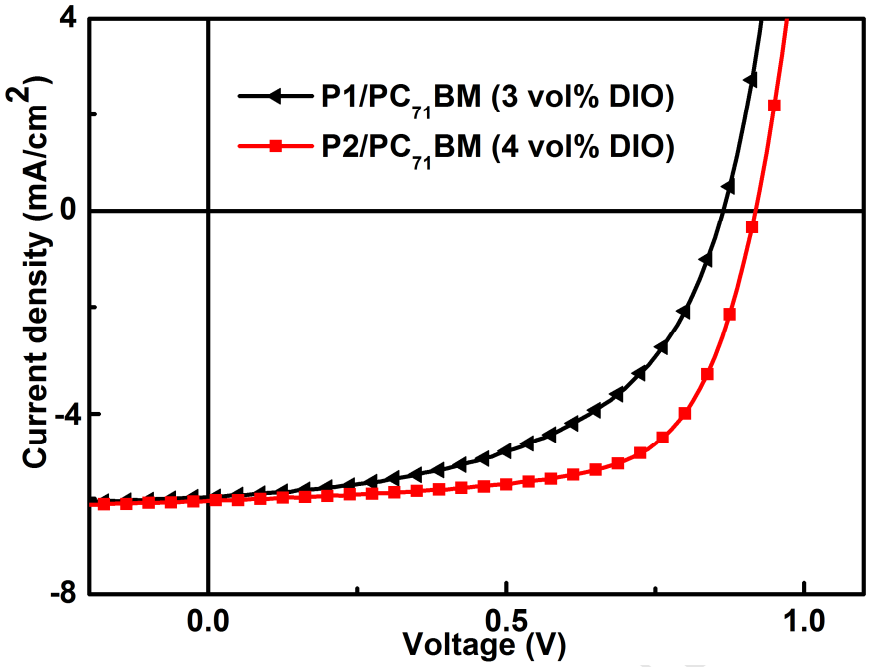

Figure 8

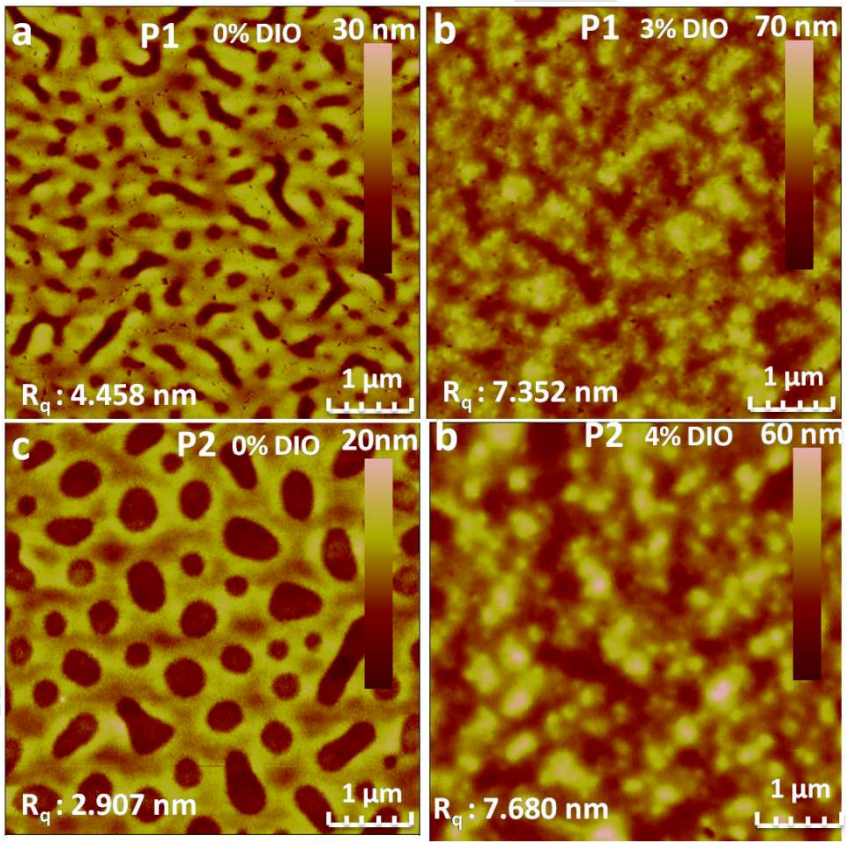

Figure 9

Table 1 Optical and redox properties of polymers.

Polymer	λ_{max}^{abs} (nm)		λ_{onset}^{abs}	E_g^{opt} [a]	HOMO[b]	LUMO[b]	E_g^{ec} [c]
	Solution	Film	Film	(ev)	(ev)	(ev)	(ev)
PBDT-PhBT [d]	462	498	627	1.98	–5.32	–3.37	–
P1	532	543	730	1.70	–5.22	–3.60	1.62
P2	536	546	730	1.70	–5.34	–3.60	1.74

[a] $E_g^{opt} = 1240/\lambda_{onset}^{abs}$ (in film). [b] HOMO = $-(4.75 + E_{onset}^{ox})$, LUMO = $-(4.75 + E_{onset}^{red})$. [c] E_g^{ec} = (HOMO − LUMO). [d] The data were referred from our previous work [13].

Table 2 Device performances of polymer/$PC_{61}BM$ solar cells.

	P1 : $PC_{61}BM$ = 1:2				P2 : $PC_{61}BM$ = 1:2			
	1%DO	2%DIO	3% DIO	4%DIO	1% DIO	2% DIO	3% DIO	4% DIO
J_{sc}/(mA.cm^{-2})	5.23	3.59	3.66	3.55	3.43	3.73	3.74	3.64
V_{oc}/V	0.60	0.81	0.81	0.81	0.80	0.74	0.77	0.79
FF	0.36	0.56	0.58	0.55	0.57	0.57	0.63	0.63
PCE/%	1.13	1.63	1.73	1.61	1.58	1.57	1.84	1.82

Table 3 Device performances of polymer/$PC_{71}BM$ solar cells.

	P1 : $PC_{71}BM$ = 1:2				**P2 : $PC_{71}BM$ = 1:2**				
	1% DIO	2% DIO	3% DIO	4% DIO	1% DIO	2% DIO	3% DIO	4% DIO	5% DIO
J_{sc}/(mA.cm^{-2})	4.76	5.69	5.96	5.95	4.41	5.08	5.97	6.04	6.16
V_{oc}/V	0.86	0.85	0.86	0.86	0.91	0.91	0.91	0.91	0.90
FF	0.55	0.52	0.53	0.48	0.61	0.66	0.67	0.66	0.62
PCE/%	2.29	2.53	2.71	2.47	2.46	3.05	3.63	3.66	3.48

Research highlights

1. Two polymers based on pyrrolo[3,4-*d*]pyridazine-5,7-dione unit were synthesized and characterized.
2. The LUMO and bandgap were lowered by introducing a more electron deficient unit.
3. The polymers maintained the deep HOMO level and the devices exhibited a PCE of 3.66% with a high V_{oc} of 0.91 V.